Supplementary Information

Ultrathin nucleoporin FG repeat films and their interaction with nuclear transport receptors

*Nico B. Eisele,[1,2] Steffen Frey,[2] Jacob Piehler,[3] Dirk Görlich,[2] and Ralf P. Richter [1,4]**

[1] Biosurfaces Unit, CIC biomaGUNE, Paseo Miramon 182, 20009 Donostia - San Sebastian, Spain

[2] Department of Cellular Logistics, Max Planck Institute for Biophysical Chemistry, Am Fassberg 11, 37077 Göttingen, Germany

[3] Department of Biology, University of Osnabrück, Barbarastraße 11, 49076 Osnabrück, Germany

[4] Max Planck Institute for Metals Research, Heisenbergstraße 3, 70569 Stuttgart, Germany

*Corresponding author. E-mail: rrichter@cicbiomagune.es. Phone: +34 943 00 5329. Fax: +34 943 00 5315

Materials and Methods

Buffer: A buffer solution of 150 mM NaCl, and 10 mM HEPES, pH 7.4, in ultrapure water was used to prepare lipid vesicles, to dilute protein stock solutions, and in all experiments reported. 5 to 25 mM $NiCl_2$ were added for the incubation step leading to the formation of a supported lipid bilayer.

Preparation of lipids and lipid vesicles: Lyophilised dioleoylphosphatidylcholine (DOPC) and dioleoylphospatidylethanolamine-CAP-biotin (DOPE-CAP-Biotin) were purchased from Avanti Polar Lipids (Alabaster, AL, USA). A lipid analogue based on a chelator headgroup comprising two nitrilotriacetic acid moieties (bis-NTA) was prepared as described earlier (Lata et al, 2006). The divalent presentation of NTA improves the binding stability of histidine-tagged proteins, with dissociation constants in the lower nM range (Lata et al, 2005).

Lipids were mixed in chloroform, dried, re-suspended in buffer and homogenised as described earlier (Richter et al, 2003). Small unilamellar vesicles (SUVs) were obtained by sonication (30 min) with a tip sonicator (Branson, USA), operated in pulsed mode at 30% duty cycle with refrigeration, followed by centrifugation in an Eppendorf centrifuge (10 min at 14,000 *g*) to remove titanium particles. SUV suspensions were stored at 4ºC under nitrogen. Concentrations and mixing ratios were estimated from the dry masses of employed lipid material. Before use vesicle suspensions were diluted to 50 µg/ml.

E. coli expression vectors: Plasmids allowed for recombinant expression of indicated proteins in *E. coli*. Complete plasmid sequences are available on request (Table S1).

Table S1: E.coli expression vectors.[a)]

Name	protein name	expressed protein	resistance conferred by plasmid	Reference
pSF345	$Nsp1^{2-601}$	His_{10}-TEV-$Nsp1^{2-601}$-Cys	Ampicillin	(Frey et al, 2006)
pSF362	$Nsp1^{2-601}$(F→S)	His_{10}-TEV-$Nsp1^{2-601}$(F→S)-Cys	Ampicillin	(Frey et al, 2006)
pSF1106	PrA-TEV-scImpβ	ProteinA-TEV-scImpβ	Kanamycin	this study
pSF970	Bio-scImpβ	His_{14}-TEV-Bio-scImpβ	Kanamycin	this study
pSF966	MBP-TEV-BirA	MBP-TEV-BirA	Spectinomycin	this study
pSF844	MBP-mCherry	His_{14}-TEV-MBP-mCherry	Kanamycin	(Frey & Görlich, 2009)
pSF807	IBB-mEGFP	His_{14}-TEV-IBB-mEGFP-Cys	Kanamycin	this study
pSF814	Gsp1p (yeast Ran)	His_{14}-TEV-Gsp1p	Kanamycin	this study
pSF815	Prp20p (yeast RCC1)	His_{14}-TEV-Prp20p	Kanamycin	this study
pSF488	His_{10}-GFP-MBP	His_{10}-GFP-MBP-Cys	Ampicillin	this study

[a)] Abbreviations: His_{10}/ His_{14}, histidine tag; TEV, TEV-protease recognition site; PrA, ProteinA; Bio, AviTag (GLNDIFEAQKIEWHE; (Schatz, 1993)); IBB, importin β-binding domain (corresponding to amino acids 2-63 of *S. cerevisiae* Srp1p).

Expression and purification of proteins: To produce His_{10}-tagged Nsp1 FG/FxFG repeat domain (M_w = 64.6 kDa) or its F→S mutant (61.3 kDa), *E. coli* transformed with pSF345 or pSF362, respectively, was grown at 37°C to OD_{600} = 2.0 in TB medium supplemented with 200 µg/ml ampicillin. The culture was cooled down to 25°C, induced with 1 mM IPTG, and further incubated for 3 h. Before cell harvest, 1 mM PMSF (phenylmethylsulfonyl fluoride) and 5 mM EDTA were added directly to the culture. Cells were resuspended in 8.3 M guanidinium-hydrochloride (Gua-HCl) containing 2 mM EDTA and 20 mM DTT and lysed by a single round of freezing and thawing. After centrifugation for 60 min at 38000 rpm, the cleared lysate was supplemented with 100 mM Tris/HCl (pH 8.5) and 1 mM imidazole and applied to a nickel-chelate column. The column was washed with 7.5 Gua-HCl, 100 mM Tris/HCl (pH 8.5), 1 mM EDTA, 1 mM imidazole followed by a second wash

step with 6 M Gua-HCl, 20 mM Tris/HCl (pH 8.0), 1 mM EDTA, 1 mM imidazole. Bound protein was eluted with 4.5 M Gua-HCl, 15 mM Tris/HCl (pH 8.0), 1 mM EDTA, 500 mM imidazole and applied to a thiopyridine-activated, SH-reactive matrix. The matrix was washed with 6 M Gua-HCl, 20 mM Tris/HCl (pH 8.0), 1 mM EDTA, 1 mM imidazole followed by a second washing step with deionised water. Proteins were eluted with 6 M Gua-HCl, 20 mM Tris/HCl (pH 7.5), 1 mM iminodiacetic acid, 10 mM DTT, applied to a preparative C18 reverse phase HPLC column, eluted with increasing concentrations of acetonitrile in 0.15 % TFA, and lyophilised. Pure proteins were dissolved in 6 M Gua-HCl, 1 mM iminodiacetic acid, 10 mM acetic adic, 5 mM sodium acetate at 460 µM (WT) and 320 µM (F→S mutant), respectively.

To produce the respective untagged proteins, the eluates from the SH-reactive matrix were transferred into 2 M urea, 50 mM Tris/HCl (pH 7.5), 2 mM EDTA, 5 mM DTT, and the His_{10}-tag was cleaved off using his-tagged TEV-protease. TEV-protease, the tag and remaining non-cut proteins were separated from the pure repeat domain by two successive passages over a nickel-chelate column. The flow-through was adjusted to 6 M Gua-HCl and applied to RP-HPLC as described before.

To produce untagged scImpβ (95.2 kDa), *E. coli* strain BLR transformed with pSF1106 was grown at 25°C to OD_{600} = 1.0 in TB medium supplemented with 50 µg/ml kanamycin. The culture was cooled down to 18°C, induced with 0.5 mM IPTG, and further incubated over night. Before cell harvest, 1 mM PMSF (phenylmethylsulfonyl fluoride) and 5 mM EDTA were added directly to the culture. Cells were resuspended in buffer HS (2 M NaCl, 50 mM Tris-HCl (pH 8.0), 5 mM $MgCl_2$, 1 mM imidazole, 0.5 mM EDTA, 10 mM DTT) and lysed by sonication. After centrifugation for 60 min at 37000 rpm, the cleared lysate was applied to IgG sepharose (GE healthcare). After extensively washing with buffer HS and buffer A (44 mM Tris-HCl (pH 7.5), 290 mM NaCl, 4.4 mM $MgCl_2$, 0.44 mM EDTA, 10 mM β-ME), bound protein was eluted by incubation with TEV protease, concentrated and further purified by gel filtration on a Superdex200 column (GE Healthcare) equilibrated with buffer A. To remove trace amounts of residual TEV protease, the peak fractions were pooled and passed through a nickel-sepharose column. The final protein preparation was supplemented with 1/9 volume 2.5 M sucrose, concentrated to 100 µM and frozen in liquid nitrogen.

To produce biotinylated scImpβ (97.3 kDa), plasmids encoding His_{14}-TEV-Bio-scImpβ and MBP-TEV-BirA were co-transformed in *E.coli* strain BLR. The cells were grown in TB medium supplemented with 50 µg/ml kanamycin, 50 µg/ml spectinomycin and 20 µg/ml biotin at 25°C. At OD_{600} = 0.4, the cultures were induced with 0.2 mM IPTG and the temperature was shifted to 20°C for 15 hours. Before harvesting the cells, 1 mM PMSF and 5 mM EDTA were added to the culture. After centrifugation and resuspension of the cell pellet in buffer HS, cells were disrupted by sonication and the lysate was cleared by centrifugation at 37000 rpm for 60 min. Cleared lysates were applied to a nickel-sepharose column equilibrated with buffer HS. After washing off unbound proteins with buffer HS followed by buffer A, proteins were eluted with buffer A supplemented with 300 mM imidazole. The his-tag was cut off with TEV protease (1:50 enzyme to substrate ratio) at room temperature. Cut proteins were further purified by gel filtration on a Superdex200 16/60 column (Pharmacia) equilibrated with buffer A followed by a second passage over nickel-sepharose. The purified protein was supplemented with 1/9 volume 2.5 M sucrose, concentrated to 100 µM and frozen in liquid nitrogen.

Expression of MBP-mCherry (67.3 kDa) was described previously (Frey & Görlich, 2009). Purification was performed as described above for biotinylated scImpβ. The stock solution had a concentration of 100 µM. IBB-mEGFP, Gsp1p and Prp20p were expressed and purified following the identical protocol.

Expression and purification of His_{10}-GFP-MBP (69.1 kDa) was performed analogous to MBP-mCherry, however, the cleavage with TEV-protease and the second passage over the nickel-sepharose column were omitted.

The scImpβ•IBB-mEGFP complex (129.6 kDa) was pre-formed using an 1.5-fold excess of IBB-mEGFP over scImpβ and purified by gel filtration on a Superdex200 16/60 column equilibrated with

buffer A. The complex was concentrated, supplemented with 1/9 volume of 2.5 M sucrose and frozen in liquid nitrogen. The stock had a concentration of 100 µM.

The scImpβ•Gsp1p•GTP (120.3 kDa) complex was formed by incubating a mixture of 45 µM Gsp1p, 20 µM scImpβ, 2 µM Prp20p, 0.4 µM pyruvate kinase, 0.5 mM GTP and 10 mM phosphoenolpyruvate in buffer A for 1.5 h at room temperature. The complex was purified by gel filtration on a Superdex200 16/60 column equilibrated with buffer A, followed by a passage over a nickel-sepharose column to remove trace amounts of his-tagged proteins. The complex was concentrated, supplemented with 1/9 volume of 2.5 M sucrose and frozen in liquid nitrogen. The stock had a concentration of 100 µM.

Lyophilised avidin (Av, 66 kDa) was purchased from Sigma, and reconstituted in ultrapure water to a concentration of approximately 15 µM, as described by the manufacturer. Before use the solution was diluted to about 0.05 µM.

Substrate preparation: Silica-coated QCM-D sensors (QSX303, Q-Sense, Gothenburg, Sweden) and silicon wafers with a native oxide layer of less than 2 nm thickness (University Wafers, South Boston, MA, USA) were cleaned by immersion in a 2% sodium dodecyl sulfate solution for 30 min, rinsing with ultrapure water, blow-drying with nitrogen, and exposure to UV/ozone (BioForce Nanosciences, Ames, IA, USA) for 30 min. Cleaned substrates were stored in air and again exposed to UV/ozone (30 min) prior to use.

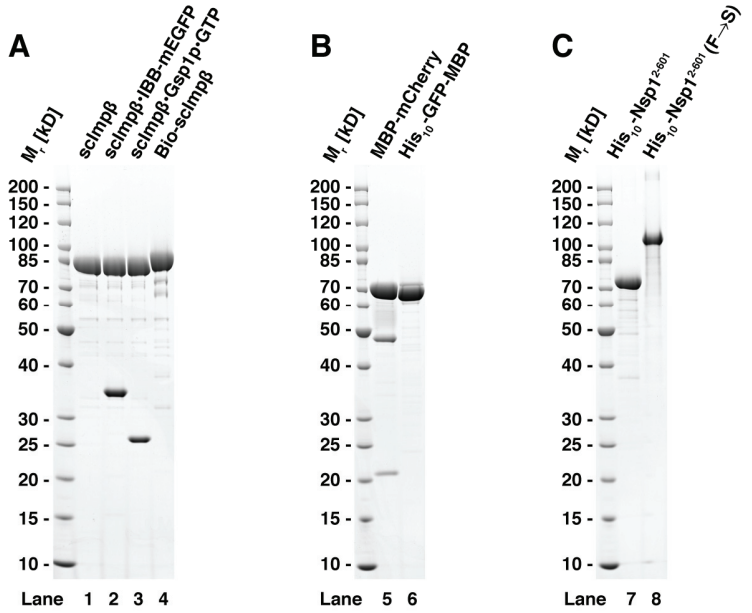

Figure S1: Quality of purified recombinant proteins used in this study. SDS PAGE of scImpβ, scImpβ complexes and biotinylated scImpβ (A), MBP fusion proteins (B) and His_{10}-tagged Nsp1 repeat domains (C). All preparations contain more than 90% full length protein. Major bands at 35 kD in lane 2 and 26 kD in lane 3 correspond to IBB-mEGFP or Gsp1p, respectively, which stoichiometrically associate with scImpβ. Minor bands at 48 kD and 21 kD in lane 5 are indicative for a specific backbone break observed during maturation of the mCherry fluorophore. This break does not influence the integrity of the MBP-mCherry fusion or its Stokes radius as judged from size exclusion chromatography.

Quartz crystal microbalance with dissipation monitoring

QCM-D measures changes in resonance frequency, Δf, and dissipation, ΔD, of a sensor crystal upon interaction of (soft) matter with its surface. The QCM-D response is sensitive to the mass (including coupled water) and the mechanical properties of the surface-bound layer. Adsorption and interfacial processes were monitored *in situ* with sub-second time resolution.

QCM-D measurements were performed with a Q-Sense E4 system (Q-Sense AB, Västra Frölunda, Sweden). The system was operated in flow mode with a rate of typically 20 µl/min, using a syringe pump (KD Scientific, Holliston, MA, USA). The working temperature was 23°C. Δf and ΔD were measured at 6 overtones ($n = 3, 5 \ldots 13$, corresponding to resonance frequencies of $f_n \approx 15, 25 \ldots 65$ MHz) simultaneously. Changes in dissipation and normalised frequency, $\Delta f = \Delta f_n/n$, of the fifth overtone are presented.

Quantification of FG repeat film thickness by QCM-D: The thickness of FG repeat monolayers was estimated by fitting the QCM-D data to a viscoelastic model (Domack et al, 1997; Voinova et al, 1999) as implemented in the software QTM (D. Johannsmann, Technical University of Clausthal, Germany). The model relates the measured QCM-D responses, Δf and ΔD as a function of n, to the viscoelastic properties of the adsorbed layer(s) and the surrounding solution. The small load approximation was employed (see (Johannsmann, 2007) for further information). The FG repeat film was represented by a viscoelastic layer with thickness d, density ρ, storage modulus G', and loss modulus G''. The storage modulus is a measure for the elasticity of the film. The loss modulus is related to the film's viscosity, η, by $G'' = 2\pi f\eta$. A material is called elastic (viscous), if $G' >> G''$ ($G' << G''$). If $G' \approx G''$, it is called viscoelastic.

The layer's density was coupled to the thickness via

$$\rho = \rho_{\text{Solution}} + \frac{m_{\text{Protein}}}{d}\left(1 - \frac{\rho_{\text{Solution}}}{\rho_{\text{Protein}}}\right), \qquad \text{(S1)}$$

with ρ_{Protein} and m_{Protein} being the protein density (1.35 g/cm^3) and the protein mass per surface area in the film, respectively. m_{Protein} was estimated by ellipsometry. The viscoelastic properties, G' and G'', were allowed to be frequency dependent, following power laws with exponents α' and α'', respectively. The exponents were allowed to vary within ranges that are physically reasonable for polymer solutions and gels, i.e., $0 \le \alpha' \le 2$ and $-1 \le \alpha'' \le 1$ (Ferry, 1980). The semi-infinite bulk solution was assumed to be Newtonian with a viscosity of 0.89 mPa·s, and a density of $\rho_{\text{Solution}} = 1.0$ g/cm^3. The SLB exhibited very low dissipation and was therefore treated as a rigid layer ("Sauerbrey layer"). All measured overtones were included in the fitting routine.

For the investigated FG repeat films, a unique fit of good quality was obtained. Fig. S2 displays the best fit to the data in Fig. 1B, and Table S2 (measurement #1) shows the corresponding results. The film thickness of 34 nm was rather well determined, with changes of less than ±15% leading to more than twofold increases in χ^2. All other parameters were also rather well constrained by the QCM-D data (Table S2). The loss modulus of about 100 kPa corresponds to a viscosity of 3.2 mPa·s, which is 3.6-fold the viscosity of water. The storage modulus of 150 kPa is similar to the elasticity of polydimethylsiloxane (PDMS) at medium cross-linker density (Brown et al, 2005). It should be noted that the viscous and/or elastic behaviour of a given material depends on the frequency at which it is deformed (Ferry, 1980). The QCM-D operates at considerably higher frequencies (MHz) than common bulk rheometers (mHz to kHz). The viscoelastic properties reported here may thus differ from those obtained by other methods.

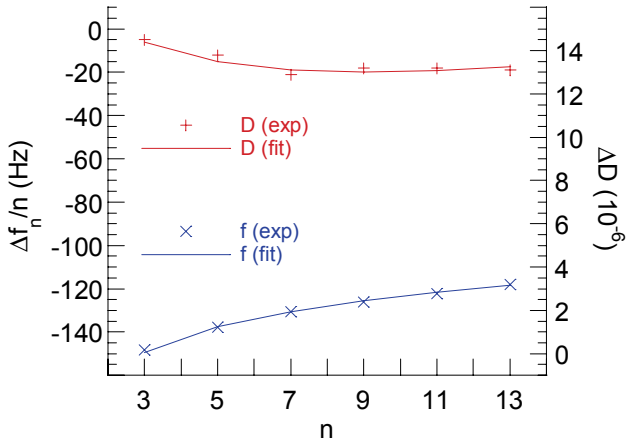

Figure S2: Experimental and fitted QCM-D responses for an FG repeat film. The data correspond to Fig. 1B (at 20 min).

Effect of scImpβ influx on the FG repeat film: The response of FG repeat films to selected bulk concentrations of scImpβ was measured by QCM-D (Fig. 4B). The thickness and viscoelastic properties of the films were quantified with the viscoelastic model, and are displayed in Table S2 (measurement #2). Note that the FG repeat film that was used in the titration assay (measurement #2) was slightly less dense than the film displayed in Fig. 1 (measurement #1), resulting in a slightly lower thickness. Upon addition of scImpβ, the thickness increased weakly, by a few nanometers at most, with increasing scImpβ concentrations. At the same time, the storage and loss moduli increased, by a few 10%, indicating moderate film rigidification. The data in Table S2 illustrate that the pronounced increase in the absolute frequency shift that is observed upon incubation of 5 μM scImpβ (Fig. 4B) stems from a combination of moderate increases in the film's hydrated mass ($d \times \rho$), elasticity (G') and viscosity (expressed in G'').

Table S2: Properties of FG repeat domain films, as determined from fits to the viscoelastic model.

measurement	$c_{scImp\beta}$	d [a)]	ρ	G' [a), b)]	α' [a)]	G'' [a), b)]	α'' [a)]
	(μM)	(nm)	(g/cm^3)	(kPa)		(kPa)	
#1	-	34±4	1.05±0.01	150±60	0.15±0.15	103±15	0.94±0.03
#2	-	29±4	1.05±0.01	96±50	0.2±0.2	93±20	0.93±0.04
	0.2	30±4	1.06±0.01	82±50	0.2±0.2	103±20	0.93±0.04
	1.0	32±4	1.07±0.01	89±50	0.2±0.2	116±30	0.93±0.04
	5.0	34±4	1.09±0.01	117±50	0.2±0.2	129±30	0.93±0.04

[a)] Errors correspond to the range within which χ^2 does not increase by more than two-fold from the value obtained for the best fit.
[b)] G' and G'' are given at f = 5 MHz.

***In situ* ellipsometry**

Ellipsometry measures changes in the ellipsometric angles, Δ and Ψ, of polarised light upon reflection at a planar surface. We employed ellipsometry *in situ*, using silicon wafers as substrates that were installed in an open cuvette with continuously stirred sample solution, to quantify adsorbed/absorbed masses in a time-resolved manner.

Data were acquired with a spectroscopic rotating compensator ellipsometer (M2000V, Woollam, NE, USA), operating in a wavelength range from λ = 380 to 1000 nm, at 70º angle of incidence and a time resolution of ~5 s, using a custom-designed open glass cuvette at ambient temperature. The cuvette setup was inspired by Corsel et al. (Corsel et al, 1986). Samples were injected directly into the buffer-filled cuvette at desired concentrations, and continuously stirred with a magnetic stirrer (~200 rpm). To remove samples, the cuvette content was diluted, by repeated addition of at least a 2-fold excess of buffer and removal of excess liquid, until the concentration of soluble sample was below 10 ng/ml. The stirrer ensured homogenisation of the cuvette content within a few seconds.

Quantitative evaluation of in situ ellipsometric data: Bound masses were determined by numerical fitting of the ellipsometric data to a multi-layer model. Ellipsometric data were fitted over the accessible wavelength spectrum, using the software CompleteEASE (Wollam, NE, USA). The model relates the measured ellipsometric responses, Δ and Ψ as a function of λ, to the optical properties of the substrate, the adsorbed layer(s) and the surrounding solution.

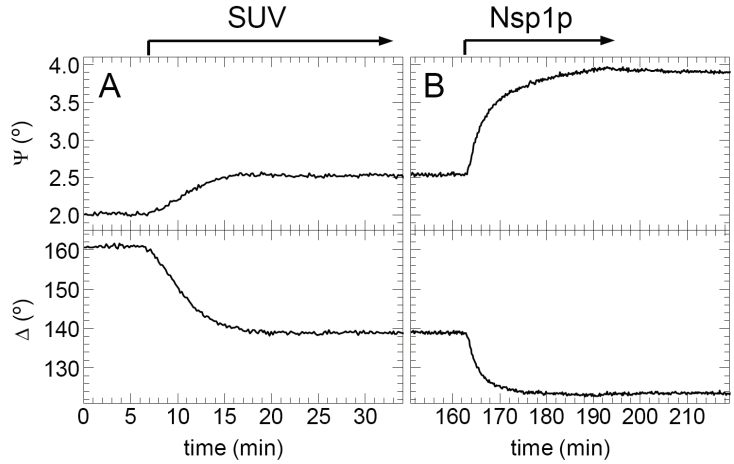

Figure S3: Representative ellipsometric data, Δ and Ψ at λ = 633 nm, for the formation of a supported lipid bilayer (*A*), and an FG repeat film (*B*).

Calibration: The cuvette was verified to exhibit negligible window effects. To this end, a calibration wafer with a silica overlayer of ~20 nm thickness (Wollam) was employed, as described by the manufacturer. Only cells were used that induced an absolute offset in Δ smaller than 0.5º.

The cleaned silicon wafers were characterised in buffer in the cuvette prior to each *in situ* measurement. The thickness and the optical properties of the silica overlayer were determined, based on a three-layer model (solvent, native silicon oxide, silicon) and tabulated optical constants for silicon (CompleteEASE, Wollam). The native oxide layer was treated as a transparent Cauchy medium, with a refractive index of $n_{oxide}(\lambda) = A_{oxide} + B_{oxide} / (\lambda/\mu m)^2$. The semi-infinite bulk solution was also treated as a transparent Cauchy medium. Its refractive index, $n_{solvent}(\lambda) = 1.325 + 0.00322 / (\lambda/\mu m)^2$, was calculated from tables in the literature (Daimon & Masumura, 2007; Lide, 2004). The measured thickness of the native oxide layer was found to be 1.9±0.2 nm. Its optical properties were $A_{oxide} = 1.472 \pm 0.013$ and $B_{oxide} = 0.020 \pm 0.003$. The χ^2-value for the best fit was typically smaller than 1.4, indicating an excellent fit.

Quantification of adsorbed amounts: To extract the properties of the adsorbed biomolecular layer from the ellipsometric response, a four-layer model (solvent, biomolecular layer, native silicon oxide, silicon) was used. The SLB and the protein film were treated as a single biomolecular layer. We assumed this layer to be transparent and homogeneous (Cauchy medium), with a given thickness, d_{bml}, and a wavelength-dependent refractive index $n_{\mathrm{bml}}(\lambda) = A_{\mathrm{bml}} + B_{\mathrm{bml}} / (\lambda/\mu\mathrm{m})^2$. B_{bml} was fixed to 0.00322, while d_{bml} and A_{bml} were fitted simultaneously. The properties of all other layers were fixed to the values determined during calibration. The χ^2-value for the best fit was typically smaller than 2.0.

Adsorbed amounts were determined according to (De Feijter et al, 1978):

$$\Gamma = \frac{m}{M_{\mathrm{W}}} = \frac{1}{M_{\mathrm{W}}} \frac{d_{\mathrm{bml}}^{(2)}\left(n_{\mathrm{bml}}^{(2)} - n_{\mathrm{solvent}}\right) - d_{\mathrm{bml}}^{(1)}\left(n_{\mathrm{bml}}^{(1)} - n_{\mathrm{solvent}}\right)}{\mathrm{d}n/\mathrm{d}c}, \tag{S2}$$

with m being the adsorbed mass per unit area, and M_{W} the molecular weight of the adsorbate. The indices (1) and (2) refer to determined values prior to and during a given incubation step, respectively. For most proteins, and within an error of less than 5%, the refractive index increment, dn/dc, is constant over the range of concentrations encountered in the reported measurements (0 to 500 mg/mL) (Bingen et al, 2008). In Eq. S2, we employed the refractive indices of the biomolecular layers at λ = 633 nm, and used a value of dn/dc = 0.180 cm^3/g for all proteins (Brandrup et al, 1989; Fasman, 1973). In practice, the errors associated with d_{bml} and n_{bml}-n_{solvent} can be rather high for the nanometre-thin films investigated here. The errors are though covariant, i.e., the product $d_{\mathrm{bml}}(n_{\mathrm{bml}}$-$n_{\mathrm{solvent}})$ and thus the adsorbed mass can be determined with good accuracy (Cuypers et al, 1983).

Quantification of mean anchor distances: To calculate the mean distance, s, between neighbouring sites of FG repeat domain anchorage we assumed hexagonal order of the anchors:

$$s^2 = \frac{2}{\sqrt{3}} \frac{1}{N_{\mathrm{A}}\Gamma}, \tag{S3}$$

with N_{A} being Avogadro's number, and Γ the amount of adsorbed FG repeat domains (in mol/cm^2).

Determination of dissociation constants: The dissociation constant, K_{D}, and the saturation limit, Γ_{max}, for the binding of scImpβ to FG repeat films was obtained from the equilibrium absorbed amounts, Γ, as a function of NTR bulk concentration, by numerical fitting to a single-component Langmuir isotherm:

$$\Gamma = \Gamma_{\mathrm{max}} \frac{[\mathrm{scImp\beta}]}{K_{\mathrm{D}} + [\mathrm{scImp\beta}]}, \tag{S4}$$

or to a two-component Langmuir isotherm:

$$\Gamma = \Gamma_{\mathrm{max}}^{(1)} \frac{[\mathrm{scImp\beta}]}{K_{\mathrm{D}}^{(1)} + [\mathrm{scImp\beta}]} + \Gamma_{\mathrm{max}}^{(2)} \frac{[\mathrm{scImp\beta}]}{K_{\mathrm{D}}^{(2)} + [\mathrm{scImp\beta}]}. \tag{S5}$$

Estimation of partition coefficients: The partition coefficient, i.e., the relative distribution of scImpβ in the film and in the bulk solution at low scImpβ concentrations, was calculated as:

$$PC = \frac{\Gamma_{\mathrm{max}}}{K_{\mathrm{D}} d}. \tag{S6}$$

Γ_{max} and K_{D} were taken from the high affinity contribution of the Langmuir isotherm, and d from the QCM-D data (Table S2).

Estimation of dissociation rate constants: Association and dissociation of scImpβ to FG repeat films occurred fast: the relaxation times for reaching binding equilibria were typically smaller than 10 s (Fig. 2A). From this observation, we deduce a lower bound for the dissociation rate constant:

$k_{off} > 0.1\ s^{-1}$. For high affinity interactions ($K_D^{(1)} = 0.36\ \mu M$), this corresponds to a lower bound of $k_{on} > 3\times10^5\ M^{-1}s^{-1}$ for the association rate constant.

Adsorption and desorption of scImpβ may be limited (i) by the transport of the molecules to the film, (ii) by the intrinsic association/dissociation rate between scImpβ and FG repeat films, and (iii) by the diffusion of scImpβ inside the film.

- *Transport limitations:* In our experimental setup (flat surface opposite a rotating stirrer), transport of molecules to the film can be adequately described by diffusion through an unstirred layer next to the surface (Hermens et al, 2004). In our setup, and for the typical size of the proteins used here, the thickness of this layer is about 20 μm. The mass transport limited adsorption rate of scImpβ can be estimated from a reference measurement of an adsorption process that is limited by mass transport and that occurs under identical stirring conditions, according to (Hermens et al, 2004):

$$\left(\frac{\partial\Gamma}{\partial t}\right)_{\text{scImp}\beta} = \left(\frac{D_{\text{scImp}\beta}}{D_{\text{ref}}}\right)^{2/3} \frac{[\text{scImp}\beta]}{[\text{ref}]}\left(\frac{\partial\Gamma}{\partial t}\right)_{\text{ref}}. \qquad \text{(S7)}$$

  We chose the adsorption of Av to a biotinylated supported lipid bilayer as the reference (data not shown). The diffusion constants, D, of scImpβ and Av were estimated from their Stokes radius to be about 55 and 70 $\mu m^2/s$, respectively. The estimated adsorption rate for [scImpβ] = 1 μM was 0.29 $pmol/cm^2/s$. For comparison, the initial adsorption rate determined from the data in Fig. 3B was 0.23 $pmol/cm^2/s$. Within the uncertainties in the employed concentrations and diffusion constants, the two values are equal, indicating that mass transport does affect binding rates of scImpβ.

- *Diffusion inside the film:* Assuming a diffusion constant of 0.1 $\mu m^2/s$ inside the film (Frey & Görlich, 2007), it would take less than 10 ms for scImpβ to diffuse across a film of 35 nm thickness. This is several orders of magnitude faster than the measured off-rate, and hence negligible.

Atomic force microscopy (AFM)

Nanoindentation and imaging were performed with a NanoWizard II AFM (JPK, Berlin, Germany) using oxide-sharpened Si_3N_4 probes (NP-S, Veeco, CA, USA) with a nominal spring constant of 0.06 N/m and a nominal apex radius below 10 nm. The AFM probes were coated with a layer of PLL(20)-g[3.5]-PEG(2) (Susos AG, Dübendorf, Switzerland), in order to limit unspecific interactions between the AFM tip and the sample (Richter & Brisson, 2005).

SLBs and FG repeat films were prepared on silicon wafers, following the same incubation steps as those established by QCM-D (Fig. 1B). Incubation was performed in still solution, with twofold increased concentrations and incubation times.

Nanoindentation assays: Force versus displacement curves were acquired in buffer solution, at approach speeds and maximal loads of typically 100 nm/s and 1 nN, respectively. We compared only force curves that were acquired with the same tip, in order to minimise the effects that variations in the shape of the AFM probe may have on indentation. Reference force curves were acquired on a control surface - an SLB that lacked FG repeat coating – before and after indentation of each FG repeat film. Only indentation series which reproducibly showed a small interaction distance (~5 nm) on naked SLBs were accepted.

Force curves were reproducible upon repeated indentation at the same spot and at different spots on the same sample. Variations in the approach speed over more than two orders of magnitude, from 100 nm/s to 20 μm/s, did not change the force curves (data not shown), indicating that viscous lateral flow of FG repeat domains on these timescales does not affect the indentation assay.

Imaging: AFM images were acquired in solution and in tapping mode, using the NanoWizard II. We employed the same type of cantilever that was used in the nanoindentation assays. The drive frequency was typically around 13 kHz, and the free amplitude of the cantilever was set to 1 V. To ensure soft approach to the sample, the setpoint amplitude was decreased manually, in steps of a few mV, until the surface could be tracked. Scan speeds of 4 to 20 μm/s were employed.

Lateral homogeneity of FG repeat films:

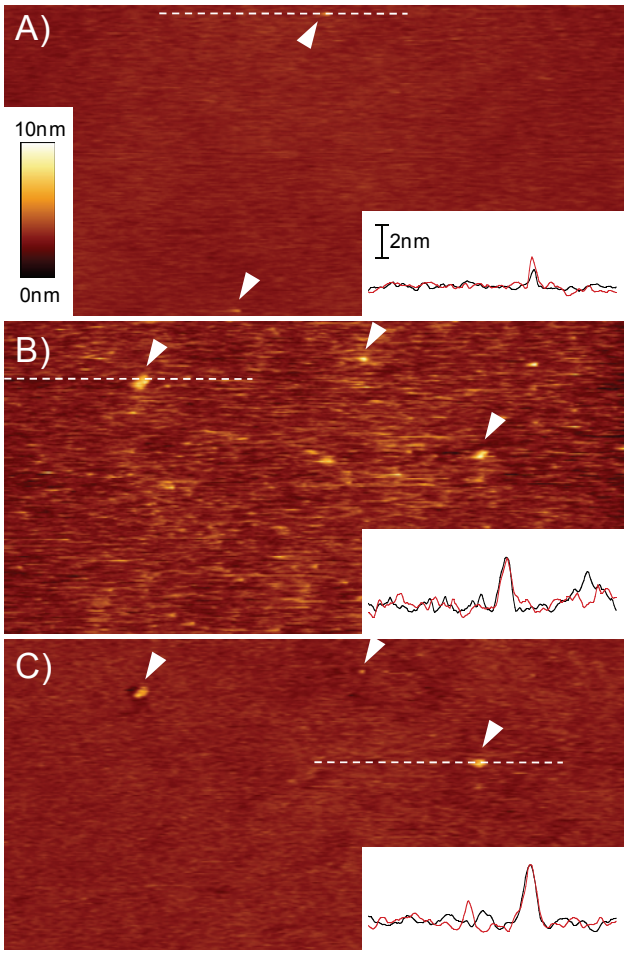

Figure S4: Representative AFM images of the surface topography of a supported lipid bilayer (*A*) and a monolayer of FG repeat domains (*B*-*C*). (*A*) Supported lipid bilayer prior to the immobilisation of FG repeat domains. Overall, the surface appears smooth. The apparent root mean square (rms) roughness is 0.2 nm. The *inset* shows the height profile of a part of a selected scan line (*white dashed line*). The Ångström-scale variations in height in the trace (*red*) and retrace (*black*) directions do not superpose well, indicating that they do not represent stable surface features but most likely experimental noise. A few defects, however, were resolved (*arrowheads*). They protruded by 2 to 5 nm out of the film, and could be stably detected upon repeated imaging of the same surface area (*not shown*). Their apparent diameter of down to 20 nm provides an upper limit for the lateral imaging resolution. These defects may represent residual vesicles that are trapped in the SLB (Richter et al, 2003). (*B*) Image of a monolayer of FG repeat domains, acquired at minimum load required for tracking the surface. The surface appears rougher than the SLB (rms roughness = 0.7 nm), although still very smooth compared to the thickness of the FG repeat film (30 to 40 nm, Fig. 4A). A comparison of trace and retrace data of a selected scan line (*inset*) shows that most of the roughness does not originate from stable surface features. Instead, it may either originate from noise and/or limited surface tracking, or from highly dynamic surface features. A few stable defects were present in the film (*arrowheads*). (*C*) Same surface area as in (*B*), imaged with slightly increased load. The apparent roughness decreases and approaches that of an SLB (rms roughness = 0.3 nm). The stable defects (*arrowheads*) remain visible, independent of the imaging load. We conclude that the FG repeat monolayers are laterally homogeneous, at least down to a length scale of a few 10 nm. Image size: 5 µm × 2.5 µm. Colour bar: false colour coding of relative heights.

Controls for the specificity of binding assays

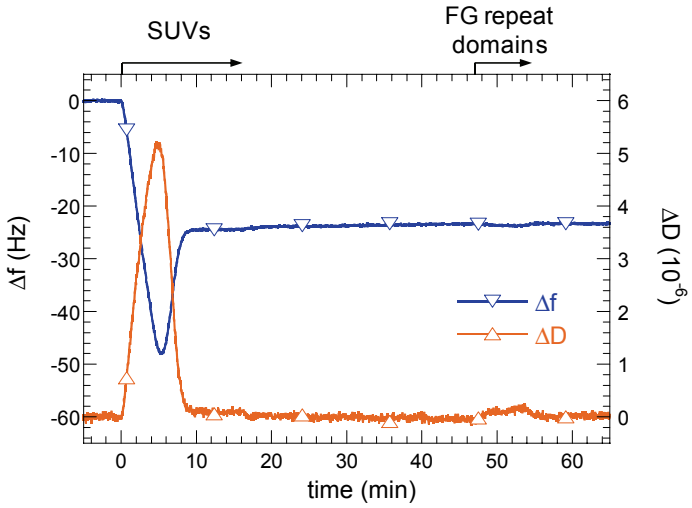

Figure S5: FG repeat domains do not bind to SLBs that lack NTA functionality. SLBs were made from 50 µg/ml SUVs containing exclusively DOPC. The QCM-D responses at the end of the incubation process were Δf = -25 Hz and $\Delta D < 0.3\times10^{-6}$, as typically observed for DOPC SLBs of good quality (Richter et al, 2003). His-tagged FG repeat domains, exposed at 3 µM concentration, induced only very small responses, $|\Delta f| < 1$ Hz and $\Delta D < 0.3\times10^{-6}$.

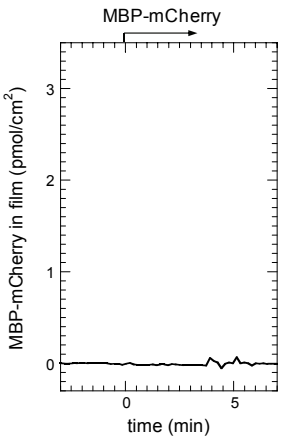

Figure S6: Binding of MBP-mCherry to an FG repeat film, monitored by ellipsometry. The FG repeat film was produced as described in Fig. 1, but with a slightly lower film density (9.1 pmol/cm^2). MBP-mCherry was incubated at a concentration of 1.1 µM. No interaction could be detected.

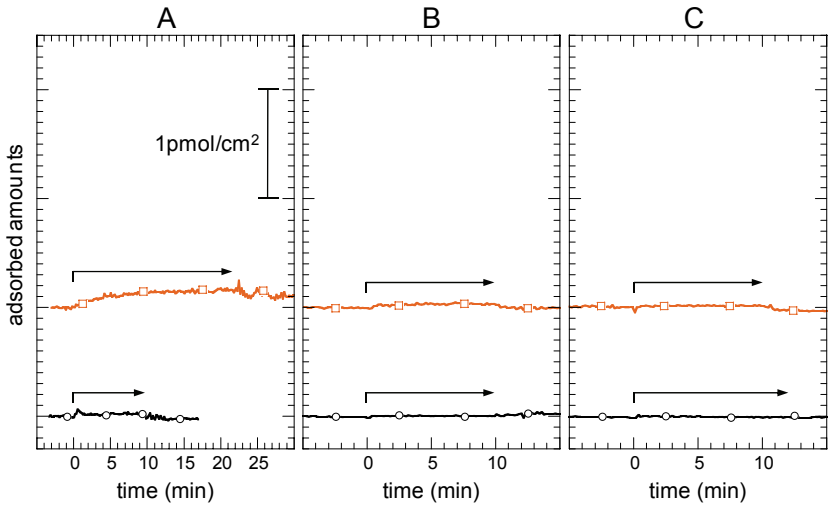

Figure S7: Controls for binding of scImpβ (*A*), scImpβ•IBB-mEGFP (*B*), and scImpβ•Gsp1p•GTP (*C*) to SLBs made of DOPC alone (black circles) and of DOPC and 10% NTA-functionalised lipids (orange rectangles). The SLBs were formed as described in Fig. S6 and Fig. 1, respectively; scImpβ, free or as a complex, was incubated at a concentration of 1 μM for the indicated durations (*arrows*). In most cases, binding was below or close to the detection limit. Some residual binding (~0.1 pmol/cm^2) was detected for scImpβ on NTA-functionalized SLBs. It is unlikely to affect the titration curve in Fig. 2 appreciably, since most of the NTA groups will be occupied by his-tags upon FG repeat film formation.

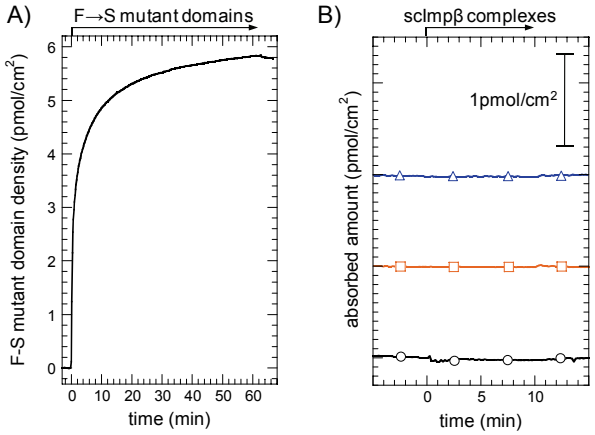

Figure S8: Interaction of scImpβ and its complexes with films that are made of a mutant form of Nsp1 FG/FxFG repeat domains in which all phenylalanines in FG context have been replaced by serines (F→S mutant, see (Frey et al, 2006) for details), monitored by ellipsometry. A NTA-functionalised SLB was formed as described in Fig. 1. His$_{10}$-tagged F→S mutant repeat domains were incubated at a concentration of 2 μM (*A*). scImpβ (*black circles*), scImpβ•IBB-mEGFP (*orange squares*), and scImpβ•Gsp1p•GTP (*blue triangles*), incubated at 1 μM concentration in solution, did not bind to the mutant film (*B*). These data confirm that the observed binding of scImpβ to FG repeat domains is specific.

All FG repeat domains in the FG repeat films are bound to the SLB

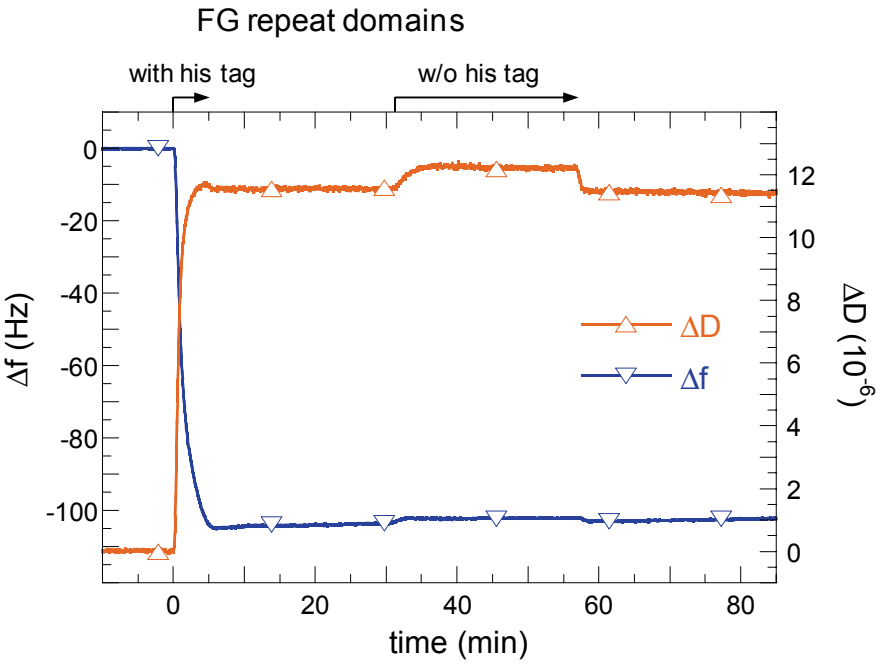

Figure S9: Interaction of his-tag free FG repeat domains with FG repeat domain films, monitored by QCM-D. A NTA-functionalised SLB was formed as described in Fig. 1. His_{10}-tagged FG repeat domains were incubated at a concentration of 3 µM, until a frequency shift of about -100 Hz was reached. Small changes in Δf and ΔD upon exposure to 3 µM his-tag free FG repeat domains may reflect changes in the film morphology due to binding of FG repeat domains. At present, we can though not exclude that they stem from minor changes in the viscosity or density of the bulk solution. Upon washing in buffer, the Δf and ΔD signals return quickly to the values prior to incubation of his-tag free FG repeat. We conclude that homophilic interactions or entanglement are not sufficient to entrap individual FG repeat domains stably in the FG repeat film. All stably bound FG repeat domains must hence be connected directly to the SLB.

Thickness of monolayers of avidin and biotinylated scImpβ

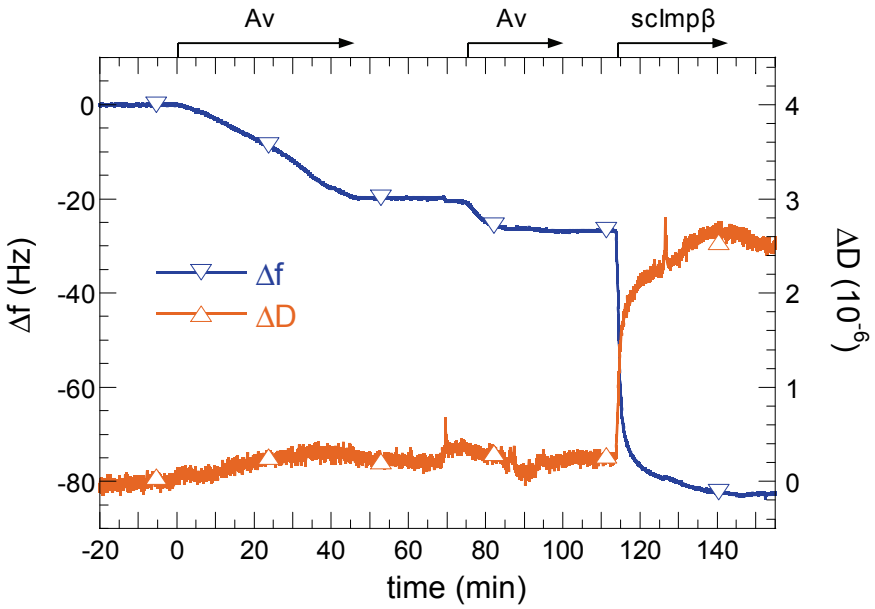

Figure S10: Formation of monolayers of avidin (Av) and biotinylated scImpβ on SLBs containing biotinylated lipids, monitored by QCM-D. The SLB was formed from 50 µg/ml SUVs containing 88 mol-% DOPC, 10% bis-NTA functionalised lipids and 2% biotin-functionalised lipids (*not shown*). Avidin was incubated in two steps, at a concentration of about 0.1 µM, until saturation. Biotinylated scImpβ was incubated at a concentration of 0.5 µM. From the final frequency shifts of -27 Hz for Av and -56 Hz for scImpβ, layer thicknesses of 4 nm and 8 nm, respectively, can be estimated, in agreement with the molecular dimensions of both molecules. For this estimate, a mean density of 1.2 g/cm^3 inside the protein layer was assumed (Bingen et al, 2008).

References

Bingen P, Wang G, Steinmetz NF, Rodahl M, Richter RP (2008) Solvation effects in the QCM-D response to biomolecular adsorption - a phenomenological approach. *Anal Chem* **80:** 8880-8890

Brandrup J, Immergut EH, Grulke EA (1989) *Polymer Handbook*, 3rd edn. New York: Wiley-Interscience.

Brown XQ, Ookawa K, Wong JY (2005) Evaluation of polydimethylsiloxane scaffolds with physiologically-relevant elastic moduli: interplay of substrate mechanics and surface chemistry effects on vascular smooth muscle cell response. *Biomaterials* **26:** 3123-9

Corsel JW, Willems GM, Kop JMM, Cuypers PA, Hermens WT (1986) The Role of Intrinsic Binding Rate and Transport Rate in the Asorption of Prothrombin, Albumin and Fibrinogen to Phospholipid Bilayers. *J Colloid Interface Sci* **111:** 544-554

Cuypers PA, Corsel JW, Janssen MP, Kop JMM, Hermens WT, Hemker HC (1983) The Adsorption of Prothrombin to Phosphatidylserine Multilayers Quantitated by Ellipsometry. *J Biol Chem* **258:** 2426-2430

Daimon M, Masumura A (2007) Measurement of the refractive index of distilled water from the near-infrared region to the ultraviolet region. *Applied Optics* **46:** 3811-3820

De Feijter JA, Benjamins J, Veer FA (1978) Ellipsometry as a Tool to Study the Adsorption Behavior of Synthetic and Biopolymers at the Air-Water Interface. *Biopolymers* **17:** 1759-1772

Domack A, Prucker O, Rühe J, Johannsmann D (1997) Swelling of a polymer brush probed with a quartz crystal resonator. *Physical Review E* **56:** 680-689

Fasman GD (1973) *Handbook of Biochemistry*, Cleveland, OH, USA: CRC Press.

Ferry JD (1980) *Viscoelastic Properties of Polymers*, 3rd edn. New York: Wiley & Sons.

Frey S, Görlich D (2007) A Saturated FG-Repeat Hydrogel Can Reproduce the Permeability Properties of Nuclear Pore Complexes. *Cell* **130:** 512-523

Frey S, Görlich D (2009) FG/FxFG as well as GLFG repeats form a selective permeability barrier with self-healing properties. *EMBO J* **28:** 2554-2567

Frey S, Richter RP, Görlich D (2006) FG-rich repeats of nuclear pore proteins form a three-dimensional meshwork with hydrogel-like properties. *Science* **314:** 815-817

Hermens WT, Benes M, Richter RP, Speijer H (2004) Effects of flow on solute exchange between fluids and supported biosurfaces. An overview. *Biotechn Appl Biochem* **39:** 277-284

Johannsmann D (2007) Studies of Viscoelasticity with the QCM. In *Piezoelectric Sensors*, Steinem C, Janshoff A (eds), Vol. 5, pp 49-110. Berlin Heidelberg: Springer

Lata S, Gavutis M, Piehler J (2006) Monitoring the Dynamics of Ligand-Receptor Complexes on Model Membranes. *J Am Chem Soc* **128:** 6-7

Lata S, Reichel A, Brock R, Tampé R, Piehler J (2005) High-Affinity Adaptors for Switchable Recognition of Histidine-Tagged Proteins. *J Am Chem Soc* **127:** 10205-10215

Lide DR (2004) *Handbook of Chemistry and Physics*, 85 edn. Boca Raton, FL, USA: CRC Press.

Richter RP, Brisson A (2005) Following the formation of supported lipid bilayers on mica - a study combining AFM, QCM-D and ellipsometry. *Biophys J* **88:** 3422-3433

Richter RP, Mukhopadhyay A, Brisson A (2003) Pathways of lipid vesicle deposition on solid surfaces: a combined QCM-D and AFM study. *Biophys J* **85:** 3035-3047

Schatz PJ (1993) Use of Peptide Libraries to Map the Substrate Specificity of a Peptide-Modifying Enzyme: A 13 Residue Consensus Peptide Specifies Biotinylation in Escherichia coli. *Nat Biotechnol* **11:** 1138-1143

Voinova MV, Rodahl M, Jonson M, Kasemo B (1999) Viscoelastic Accoustic Response of Layered Polymer Films at Fluid-Solid Interfaces: Continuum Mechanics Approach. *Physica Scripta* **59:** 391-396